Study of relativistic bound state wave functions in quasielastic $(e, e'p)$ reactions

S. Ulrych and H. Müther

Institut für Theoretische Physik, Universität Tübingen, D-72076 Tübingen, Germany

Abstract

The unpolarized response functions of the quasielastic $^{16}O(e, e'p)^{15}N$ reaction are calculated for three different types of relativistic bound state wave functions. The wave functions are obtained from relativistic Hartree, relativistic Hartree-Fock and density dependent relativistic Hartree calculations that reproduce the experimental rms charge radius of ^{16}O. The sensitivity of the unpolarized response functions to the single particle structure of the different models is investigated in the relativistic plane wave impulse approximation. Redistributions of the momentum dependence in the longitudinal and transverse response function can be related to the binding energy of the single particle states. The interference responses R_{LT} and R_{TT} reveal a strong sensitivity to the small component of the relativistic bound state wave function.

PACS number(s): 21.30.Fe, 21.60.Jz, 24.10.Jv, 25.30.Fj

I. INTRODUCTION

The exclusive $(e, e'p)$ proton knockout reaction is a powerful tool for the investigation of the single particle structure of complex nuclei [1–3]. Quasiparticle properties, such as occupation probabilities, spectroscopic factors, binding energies and momentum distributions can be determined and compared to the results of theoretical models, which have to include both, information about the electromagnetic reaction mechanism and the wave function of the bound nucleon.

The nuclear structure contributions can be seen e.g. in the reduced cross section. In the nonrelativistic plane wave impulse approximation, the reduced cross section is proportional to the momentum distribution of a single bound proton inside the nucleus. This proportionality is characterized by the spectroscopic factor, which corresponds to the probability that a single particle state is occupied by a nucleon. Therefore, spectroscopic factors can be extracted comparing experimental scattering data with theoretical predictions for the momentum distribution of the nucleus. In a mean field calculation the spectroscopic factor is equal to one for occupied or zero for unoccupied states, respectively. Different spectroscopic factors indicate the deviation from the shell model picture and therefore the importance of nucleon-nucleon correlations.

The theoretical background of the scattering formalism is provided by quantum electrodynamics, a complete relativistic framework, which describes the electromagnetic interaction with highest accuracy. Consequently, all contributions to the scattering amplitude especially the hadronic current operator are relativistic expressions and the matrix elements of the current should be calculated between states obtained from a relativistic treatment of the many-body problem. Due to the higher complexity of the relativistic problem the solution of a nonrelativistic reduction is more economic and it is able to reproduce the experimental data in a wide range of missing energies and momenta.

Relativistic calculations of exclusive $(e, e'p)$ scattering reactions, including electron distortion and final state interactions, have been performed [4–6]. The results provided spectroscopic factors e.g. for the $3s_{1/2}$ and $2d_{1/2}$ shells in ^{208}Pb of $S_\alpha \simeq 0.7$, consistent with earlier theoretical predictions. Though these spectroscopic factors are extracted from the low p_m data $(p_m \leq 300 MeV)$, relativistic calculations can give simultaneously a good reproduction of the high p_m data [7], where the main effects arise from the improved relativistic treatment of the electron distortion and the final state interaction.

The inclusion of electron distortion and final state interactions can give a good description of the experimental data, but for a deeper understanding of the relativistic reaction mechanisms the relativistic plane wave impuls approximation (RPWIA) seems to be an appropriate calculation scheme. Recently, the RPWIA was chosen to study the role of the negative energy components of the bound nucleon wave functions [8]. Analyzing the factorization of the scattering cross section, a feature of the nonrelativistic limit, the importance of relativistic effects for different choices of current operators, kinematics and restorations of current conservation has been investigated thoroughly. All calculations were made using

the bound state wave function of Horowitz and Serot [9–11]. Therefore it is interesting to ask, what influence on the results can be observed, if bound state wave functions from other relativistic nuclear structure calculations are considered. This question shall be studied in this paper.

For the investigation bound state wave functions from three different approaches were chosen, namely, the Relativistic Hartree (RH) approach of Horowitz and Serot [9–11], the Relativistic Hartree-Fock calculations (RHF) of Bouyssy *et al.* [12] and a Density Dependent Hartree (RDDH) approach including rearrangement terms of Fuchs and Lenske [13]. Each of them was used to calculate the response functions of the $^{16}O(e, e'p)^{16}N$ electron scattering reaction.

All models used are based on a microscopic understanding of the nucleus using neutrons and protons as effective degrees of freedom and the exchange of σ-, ω-, ρ- and, in the RHF approximation, π-mesons to mediate the nuclear force. They provide a consistent mathematical description starting from a covariant Lagrangian. In these models the most important contributions to the nucleon-nucleon potential arise from an attractive σ-meson exchange, which is understood as a parametrization of the 2π exchange diagrams, and a repulsive ω-meson. Calculations in finite nuclei within the mean field approximation are characterized by two large potentials of scalar and vector type (S-V) cancelling each other to a large amount. As a result the spin orbit splitting emerges automatically.

The RH and the RHF approaches use phenomenological one boson potentials. In both models the model parameters are determined in essentially the same way. The σ-N and ω-N coupling constants and the σ-meson mass were fixed in both cases to reproduce the saturation point in nuclear matter and the charge rms radius of ^{16}O.

The third model is the RDDH approximation, which is a first step to the relativistic description of finite nuclei using realistic forces. In the RDDH approximation the relativistic Brueckner-Hartree-Fock (RBHF) potential of a realistic interaction (G matrix) is parametrized in nuclear matter in terms of density dependent coupling constants and the parametrized interaction is then applied to finite systems. This calculation scheme can be regarded as a reliable approximation for the self consistent solution of the relativistic Brueckner-Hartree-Fock equations in finite nuclei [14]. RDDH calculations were performed by Brockmann and Toki [15]. It was extended to the Hartree-Fock approximation by Fritz and Müther [16] and Boersma and Malfliet [17]. In the work presented here, we use bound state wave functions from the vector density dependent RDDH approach of Ref. [13]. This many body approximation accounts for additional rearrangement terms arising from the field theoretical argument that the density dependent coupling constants have to be considered as functionals of the baryon fields. Due to the rearrangement terms this model goes beyond an effective Brueckner Hartree-Fock approximation. The model was chosen from other RDDH calculations due to its good results for the single particle as well as the bulk properties of ^{16}O.

The results for the three nuclear structure calculations yield essentially identical results for

the charge radii of ^{16}O, but have a different single particle structure. The single particle structure can be tested directly with $(e, e'p)$ knockout reactions. Using this reaction we want to investigate the sensitivity of the unpolarized response functions in the RPWIA to the model functions and to relativistic effects included in the bound state wave functions of the three approaches.

II. ELECTRON SCATTERING OBSERVABLES

As stated in section I, the theoretical description has to account for the scattering formalism as well as for the description of finite nucleon systems. In the following section the theory will be summarized, which is needed for the electron scattering observables calculated in the present work. The theoretical foundations for exclusive electron scattering reactions were developed in several publications [18]- [25]. The present paper follows the conventions of [25] except to some changes in the notation. The nuclear information is included in the matrix elements of the hadronic current

$$J^\mu(q) = \langle\, p_x s_x, \psi_{fP_B} \,|\, \hat{J}^\mu(q) \,|\, \psi_{iP_A} \,\rangle \,. \tag{1}$$

The initial state ψ_{iP_A} describes the A particle target nucleus with the four momentum $P_A^\mu = (M_A, \mathbf{0})$, whereas the final state consists of the $A - 1$ particle residual nucleus ψ_{fP_B} $(P_B^\mu = (E_B, \mathbf{p}_B))$ and the ejected proton $(p_x^\mu = (E_x, \mathbf{p}_x))$. The present investigation will be performed in the RPWIA, i.e., the outgoing proton is represented by a plane wave $\overline{u}(\mathbf{p}_x, s_x)$ and the current is given by the current of an individual constituent, treated as a free particle. The full complexity of the initial and outgoing states for the bound nucleon system is therefore replaced by a single shell model wave function $\psi_\alpha(\mathbf{p})$. In this approximation one can write for the above current matrix elements

$$J^\mu(q) = \overline{u}(\mathbf{p}_x, s_x)\hat{J}^\mu(q)\psi_\alpha(\mathbf{p}) \,. \tag{2}$$

The calculation is done completely in momentum space. The bound state wave function $\psi_\alpha(\mathbf{p})$ for the initial state is the information we obtain from the shell model calculations and $\mathbf{p} = \mathbf{p}_m$ corresponds to the missing momentum. The results of the approximation, neglecting proton and electron distortion, should not be compared to the experimental data. This approximation, however, should allow us to study the sensitivity of the results on the model for the bound state wave function $\psi_\alpha(\mathbf{p})$.

In the present investigation the main attention will be paid to the response functions, which are directly related to the hadronic tensor. If polarization is not taken into account for the incoming electron beam, as well as for the target and the outgoing particles, we can define the hadronic tensor including an average over the initial states and a sum over the final states

$$W^{\mu\nu} = \overline{\sum_i} \,\,\sum_f \!\!\!\!\!\! \diagup \,\, \delta(\epsilon_f - \epsilon_i - \omega) \, J^{*\mu}(q) \, J^\nu(q) \,. \tag{3}$$

In this definition an integration over the momentum conserving delta function has already been performed, which provides the relation $\boldsymbol{q} = \boldsymbol{p}_x - \boldsymbol{p}$. The response functions can be constructed using the hadronic tensor according to

$$
\begin{aligned}
R_L &= \int_{line} d\epsilon_{p_x} \, W^{00} \,, \\
R_T &= \int_{line} d\epsilon_{p_x} \left(W^{11} + W^{22} \right) \,, \\
R_{LT} \cos \phi &= \int_{line} d\epsilon_{p_x} \left(-W^{01} - W^{10} \right) \,, \\
R_{TT} \cos 2\phi &= \int_{line} d\epsilon_{p_x} \left(W^{11} - W^{22} \right) \,,
\end{aligned}
\tag{4}
$$

including an integration over a linewidth in the missing energy spectrum. These response functions can be used to express the unpolarized scattering cross section as a contraction of hadronic responses and the appropriate electron contributions, which are defined as in [3,21]

$$
\frac{d\sigma}{d\epsilon_{k'} d\Omega_{k'} d\Omega_{p_x}} = \frac{m |\boldsymbol{p}_x|}{(2\pi)^3} \, \sigma_M \left(V_L R_L + V_T R_T + V_{LT} R_{LT} \cos \phi + V_{TT} R_{TT} \cos 2\phi \right) \,.
\tag{5}
$$

Since recoil effects of the residual nucleus will not be considered in the present work, an appropriate factor has been neglected in the above formula. Using the definitions of this section the observables depend, except to the bound state wave function, on standard expressions like the current operator or the Dirac spinor.

III. RELATIVISTIC BOUND STATE WAVE FUNCTIONS

It was shown in the last section that the information for the calculation of the current matrix elements, which is required from relativistic nuclear structure calculations, is the momentum space wave function $\Psi_\alpha(\boldsymbol{p})$ of a particular shell model state α. The solutions of a relativistic Hartree or Hartree-Fock calculation in finite nuclei are usually given in coordinate space. The corresponding momentum space wave function can be obtained by a Fourier transformation according to

$$
\Psi_\alpha(\boldsymbol{p}) = \frac{1}{(2\pi)^{3/2}} \int d^3\boldsymbol{r} \, e^{-i\boldsymbol{p}\cdot\boldsymbol{r}} \Psi_\alpha(\boldsymbol{r}) \,.
\tag{6}
$$

More details about the bound state wave functions are given in Appendix A. In the context of $(e, e'p)$ scattering calculations a nuclear structure model should provide a good reproduction of the charge distribution, which can be observed directly in electron scattering experiments at lower energies. The three nuclear structure models chosen for the investigation here satisfy this boundary condition. We want to study the influence of the different single particle structure of these models on the unpolarized response functions of Eq. (4).

The models we use for the study are the relativistic Hartree approximation (RH) of Ref. [10], the relativistic Hartree-Fock (RHF) approximation of Ref. [12] and the density dependent

5

Hartree (RDDH) approximation of Ref. [13].

The RH and the RHF models follow the same way to fix their free parameters. The σ-N and ω-N coupling constants and the σ-meson mass are adjusted to reproduce both, the saturation point of nuclear matter and the charge rms radius of ^{16}O.

In the Hartree-Fock approximation the Dirac structure of the nucleon self energy $\Sigma(r)$ is modified due to the nonlocal structure of the two particle interaction. The self energy $\Sigma(r)$, which incorporates the influence of all other nucleons in the nucleus on a single particle, is included in the free Dirac equation according to

$$(i\partial_\mu \gamma^\mu - m - \Sigma(r))\Psi_\alpha(\boldsymbol{r}) = 0 \; . \tag{7}$$

In a nuclear system, which is characterised by rotational invariance, parity conservation and time reversal invariance, the general structure of self energy is given by

$$\Sigma(r) = \Sigma_s(r) - \gamma_0 \Sigma_0(r) + \boldsymbol{\gamma} \cdot \boldsymbol{\Sigma}_v(r) \; . \tag{8}$$

In the Hartree approximation the spatial part of the vector self energy $\boldsymbol{\Sigma}_v$ vanishes. The remaining structure is normally considered as a potential of scalar and vector (S-V) type. In the Hartree-Fock approximation the additional $\boldsymbol{\Sigma}_v$ term arises and gives a structural modification compared to the mean field approximation.

In the Hartree-Fock calculations the potentials are not given in the separated form of Eq. (8). In principle, the Dirac structure can be projected out if the Fock contributions are redefined in terms of local single particle potentials [12] and incorporated in the Dirac equation. From the nuclear matter calculations we know, that in the Hartree-Fock approximation, every meson contributes to Σ_s, Σ_0 and $\boldsymbol{\Sigma}_v$, and that the $\boldsymbol{\Sigma}_v$ term is small. This should remain true also in finite systems.

The models for the Hartree and the Hartree-Fock approximation are described by the following parameter sets: The σ-meson mass, especially sensitive to the rms radius, is chosen as $m_\sigma = 520$ MeV for the RH model [10] and $m_\sigma = 440$ MeV for the RHF model [12]. The coupling constants g_σ and g_ω were fixed to reproduce the saturation point in nuclear matter. In the RH as well as the RHF model the masses of the ω- and ρ-meson are $m_\omega = 783$ MeV and $m_\rho = 770$ MeV in accordance with the experimental values. In the RH model [10] the ρ-meson coupling constant $g_\rho^2/4\pi = 5.19$ is fixed to yield a bulk symmetry energy of 35 MeV. For the Hartree-Fock calculation we have chosen the parameter set (e) of Ref. [12], which provides the best results for the bulk and single particle properties of ^{16}O. In this set the π-N and ρ-N coupling constants of the Hartree-Fock calculations were fixed to the physical values $f_\pi^2/4\pi = 0.08$ and $g_\rho^2/4\pi = 0.55$, where a ratio of $f_\rho/g_\rho = 3.7$ for the tensor coupling of the ρ-meson was chosen. The π-meson mass in this model is $m_\pi = 138$ MeV.

For the effective relativistic Brueckner-Hartree-Fock calculation in finite nuclei we have chosen the vector density dependent (VDD) Hartree approach of Ref. [13]. Here, for the ω-meson and ρ-meson mass as well as for the ρ-meson coupling constant, the values of [10] were adopted. For the σ-meson $m_\sigma = 550$ MeV was used. The coupling constants g_σ and

g_ω were taken from a parametrization of the nuclear matter DBHF self energies [26] with second order polynomials [27].

The single particle and bulk properties of the three models, which provide the bound state wave functions needed in the electron scattering calculations, are summarized in Tab. I. The calculated energy per nucleon has been corrected in the RH and RHF models to account for the effects of the spurious center of mass motion. A contribution of 0.67 MeV has been added to the binding energy. In the RDDH model the results of Ref. [13] include already the center of mass motion. Since the calculations for the RH and the RHF approach have been performed with the computer code developed by Fritz and Müther [16], the results of Tab. I differ slightly from the original values given in the Refs. [10,12] due to numerical uncertainities. In the calculation scheme of Ref. [16] the Hartree or Hartree-Fock Hamiltonian is diagonalized in a box basis.

IV. BOUND STATES AND RESPONSE FUNCTIONS

The reaction considered in the present investigation is the proton knockout reaction $^{16}O(e,e'p)^{15}N$, where the residual nucleus is left in its ground state, i.e. the proton is knocked out of the $p_{1/2}$ state of ^{16}O.

To calculate the response functions of the $(e,e'p)$ reaction the bound state wave functions of the three models discussed above were used. The computations have been performed completely in momentum space. A new computer code has been developed. Note, that for the definition of our interference response functions in Eq. (4) we use a different convention. For the calculation of the knockout reaction we have chosen perpendicular kinematics, which provides us with the interference terms of the relativistic response functions R_{LT} and R_{TT}. For the current operator we take the CC1 description [28], using the common dipol form factors [3]. It was shown that this operator gives a simultaneous good description for high as well as low missing momenta [7] in ^{208}Pb. Furthermore, this operator enhances the contributions from the negative energy projections of the bound state wave functions as stated in Ref. [8]. For the four momentum transfer $q^\mu = k^\mu - k'^\mu = (\omega, \boldsymbol{q})$ we take kinematics I of Ref. [8] with

$$|\boldsymbol{q}| = 500 \text{ MeV/c} \qquad \omega = 131.56 \text{ MeV} , \qquad (9)$$

where the value of ω corrsponds to the quasielastic peak value ω_{QE}. Note, that for the definition of our interference response functions in Eq. (4) we use a different convention.

The response functions for the three models presented in the last section are displayed in Fig. 1. On the upper left panel we see the longitudinal response function R_L. In all figures the results obtained from RH bound state wave functions are displayed with solid lines, whereas the RHF and the RDDH results are displayed with dash-dotted and dashed lines, respectively. It can be observed that the maximal strength of R_L is reduced by the RHF and the RDDH approach in the order of 10% relative to the RH approach.

The integrated strength of the response functions

$$I_i = \int dp_m p_m^2 R_i(p_m) \;, \tag{10}$$

$(i = L, T, LT, TT)$ shows if either a reduction corresponds to a redistribution of the strength in momentum space or there occurs a true reduction of the strength. The results for the integrations are displayed in Tab. II. For the longitudinal response function one finds values of $I_L = 2.81$ for the RDDH and $I_L = 2.83$ in the case of the RH and the RHF approach, where the factor 100 has been multiplied to the original values. Therefore, the reduction of the maxima can be understood essentially as a redistribution of the total strength over the momentum scale, leading to higher values in the RHF and RDDH response functions for large p_m.

For the transversal response R_T displayed in the upper right panel of Fig. 1 a similar behaviour as for R_L is found considering the RH and the RHF bound state wave functions. However, the response function R_T obtained from the RDDH bound state wave functions shows a stronger reduction relative to the other transversal responses. This becomes more obvious, if we consider the integrated strength, which takes $I_T = 3.30$ for the RH and $I_T = 3.31$ for the RHF response, whereas for the RDDH approach we find $I_T = 3.12$.

In the interference contributions this integral reduction can be observed as well. In addition a small reduction is induced by the RH wave functions compared to the response R_{LT} of the RHF wave functions, which is reflected by a smaller value of I_{LT}. This reduction is even enhanced in the R_{TT} response. Note, that the maximum values arising from the RH wave functions are larger. That means we have an additional enhancement of the large momentum components in the RHF transverse responses arising from the increased total strength, which is not so obvious in Fig. 1.

In order to summarize these features, one may say that we observe two effects

- a redistribution of the strength of the response functions from lower momenta to high missing momenta if we compare results derived from RH, RHF and RDDH, respectively.

- a reduction of the integrated strength if we compare the results of RH and RHF on one side with these derived from RDDH on the other side. This reduction is negligible for the longitudinal response R_L, but significant for the response functions R_{LT} and R_{TT}.

In order to understand the redistribution of the strength in the example of the longitudinal response R_L, we consider the single particle densities of the three models in the momentum and the coordinate space. The single particle density is defined in momentum space according to

$$
\begin{aligned}
n_\alpha(p) &= \frac{2j_\alpha + 1}{4\pi} \int d\Omega_p \, \overline{\Psi}_\alpha(\boldsymbol{p}) \gamma_0 \Psi_\alpha(\boldsymbol{p}) \\
&= \frac{2j_\alpha + 1}{4\pi} \left(g_\alpha^2(p) + f_\alpha^2(p) \right) \;,
\end{aligned} \tag{11}
$$

8

where the upper and lower components of the relativistic wave functions, $g_\alpha(p)$ and $f_\alpha(p)$, are defined in Appendix A. The density in coordinate space is defined in analogy to Eq. (11) with the Fourier transformed expressions. The densities are normalized to the number of particles in a particular shell α.

On the left panel of Fig. 2 the density in coordinate space multiplied with the square of the radius, $r^2 n_{p1/2}(r)$, is shown. For this expression the area below the curves is identical for the three different models. The density $n_{p1/2}(r)$ itself shows an analog but inverse behaviour as the longitudinal response function R_L. The function $r^2 n_{p1/2}(r)$ indicates that the single particle densities of the RHF and the RDDH approaches are shifted to smaller radii. This is the reason of the higher momentum components in the wave functions. Though the shift in the radial wave functions is small, we have seen that this leads to a 10% reduction of the maxima of R_L. This redistribution of the momentum distribution and density distribution in configuration space is also connected to the single particle energy of the $p1/2$ state (see table I). This state is most weakly bound in the RH approximation. Therefore it is less localized in configuration space and the momentum distribution of this state is shifted to smaller momenta in this approach as compared to the other calculations.

In the nonrelativistic PWIA the momentum density of a single particle state is proportional to the reduced cross section. On the right panel of Fig. 2 the momentum density $n_{p1/2}(p_m)$ is shown in a logarithmic scale, which emphasizes the high momentum contributions. Corresponding to the longitudinal response function the maxima of $n_{p1/2}(p_m)$ are reduced starting from $n_{p1/2}^{max} = 83.3$ for the RH wave functions to $n_{p1/2}^{max} = 74.8$ respectively $n_{p1/2}^{max} = 73.0$ for the RHF and the RDDH wave functions (all values in $[(GeV/c)^{-3}]$). The numerical values show that the behaviour of the momentum density explains the structure of the response function R_L. In Fig. 3 we can see in addition that the upper component of the bound state wave function $g_{p1/2}(p_m)$ already reflects the typical momentum distribution of R_L.

In the RH and the RHF responses beside the effects arising from the different single particle densities no significant differences can be observed. The Σ_v term, included in the RHF potential, can therefore be expected to give no substantial modification of the response functions.

The reduction of the integrated RDDH responses R_T, R_{LT} and R_{TT} has another origin. This reduction is closely related to the lower component of the bound state wave function f_α. In relativistic nuclear structure calculations this small component is enhanced as compared to a small component which just arises from a boost of a nucleon with mass m. In order to explore the sensitivity we compare results of the relativistic calculation, with those in which this enhancement of the small component is suppressed. This nonrelativistic limit $\Psi_\alpha^{nr}(\boldsymbol{p})$ of the bound state wave function is defined as

$$g_\alpha^{nr}(p) = N^{nr} g_\alpha(p) \qquad\qquad f_\alpha^{nr}(p) = N^{nr} \frac{p}{E_p + m}\, g_\alpha(p)\ , \qquad\qquad (12)$$

where N^{nr} is a normalisation constant and $E_p = \sqrt{p^2 + m^2}$. The small component $f_\alpha^{nr}(p)$ is just a result of boosting the single particle spinor and therefore of pure kinematical origin.

9

This definition (12) means that the momentum dependence of the lower component $f_\alpha^{nr}(p)$ is given, except to a relativistic factor, by the upper component $g_\alpha(p)$ of the relativistic wave function. On the right panel of Fig. 3 the upper component of this nonrelativistic limit is shown. The relativistic upper component $g_{p1/2}(p)$ is slightly smaller than than the nonrelativistic $g_{p1/2}^{nr}(p)$ due to the normalisation constants N^{nr}. The situation is completely different for the lower component $f_{p1/2}(p)$, which is displayed on the left panel of Fig. 4. We find an enhancement of approximately 60% compared to the nonrelativistic wave function $f_{p1/2}^{nr}(p)$ shown on the right panel of Fig. 4. This enhancement of the lower component for relativistic nucleons in the medium is consistent with the results found in nuclear matter, where the enhancement of the lower component of the Dirac spinor is characterized by an effective mass of approximately $m^* = m + U_S = 600$ MeV compared to $m = 938.9$ MeV for free nucleons. This additional medium dependence is typical for relativistic calculations and it is not included in a nonrelativistic reduction.

For the relativistic lower component $f_{p1/2}(p)$, the bound state wave function of the RDDH approach differs significantly from the lower components of the two other approaches. This indicates that the scalar potential U_S of the RDDH calculations is less attractive. We have seen that in the interference response functions R_{LT} and R_{TT}, shown in Fig. 1, these differences modify the results notably, whereas the transversal response function R_T shows small changes, since it is dominated by the upper component of the bound state wave function.

The sensitivity of the interference responses on relativistic effects in the bound state wave functions can also be demonstrated if the response functions are calculated in the nonrelativistic limit. This is shown in Fig. 5. A strong reduction especially in the reponses R_{LT} and R_{TT} can be observed. The strong dependence on the lower component has already been shown in Ref. [8]. In addition, we can see here that the model dependent information, included in the lower component, disappears. The differences of the RDDH responses compared to the other approaches are strongly reduced. The same effect as discussed above can be observed in the nonrelativistic limit of the RDDH lower component $f_{p1/2}^{nr}(p)$ displayed in Fig. 4. In this case the lower components now simply reflect the behaviour of the upper components.

In order to learn more about the typical structure of bound state wave functions, the calculations have also been performed with the density dependent models of Fritz and Müther [16]. This calculation scheme provides a good description of the binding energies, whereas the charge radii are too small. The wave functions are therefore inadequate for a study in the context of $(e, e'p)$ reactions and the results are not presented in detail. Nevertheless, two additional informations can be obtained from these calculations. The same structural difference of the longitudinal response R_L has been found between the Hartree and the Hartree-Fock approximation. A reduction of the maxima of approximately 10% and larger high momentum components. This can also be traced back to a different single particle structure. Furthermore, no reduction in the lower component of the wave function can been observed, i.e., the reduction in the RDDH approach of Ref. [13] is due to the rearrangement

terms and not part of the density dependent approach.

V. SUMMARY AND CONCLUSIONS

Bound state wave functions obtained from a relativistic Hartree, Hartree-Fock and a density dependent Hartree approach were compared and the influence on the unpolarized response functions of the $^{16}O(e,e'p)^{15}N$ reaction was studied. The nuclear structure models chosen reproduce the experimental charge radius of ^{16}O. It was therefore possible to study the sensitivity of the response functions to the different single particle structure provided by the models. The aim of this investigation is to give an estimate of possible uncertainities in the response functions and to show the influence of the additional information provided by a relativistic treatment of the many body problem.

The calculations were performed in the relativistic plane wave impulse approximation, where modifications of the results can clearly be assigned to the bound state wave functions. Comparing the three models the maxima of the R_L and R_T responses differ by $10\% - 15\%$. This reduction of the RHF and the RDDH response functions is accompanied by an enhancement at larger missing momenta, so that the integrated strength remains unchanged. This behaviour can be connected with the density distribution of the single particle states reflecting the single particle binding energies. The vector self energy Σ_v, which appears in the Hartree-Fock approximation, has no significant influence on the structure of the response functions. This result was expected, since in nuclear matter calculations its contributions are found to be small.

The interference responses R_{LT} and R_{TT} are known to be sensitive to the lower component of the relativistic bound state wave function. The RDDH lower component is significantly reduced compared to the wave functions of the other models. This reduction is clearly measured by the interference responses and influences also the integrated strengths of the response functions. The maxima of R_{LT} and R_{TT} even show a variation of around 20%. In the nonrelativistic limit this model dependent information is lost and only small differences for the interference responses can be observed. Especially, the interference responses are therefore sensitive to a complete relativistic description of the nuclear structure problem and can be used to test different relativistic approximation schemes of nuclear many body systems.

REFERENCES

[1] S. Frullani and J. Mougey, Adv. Nucl. Phys. **14**, 1 (1985).

[2] S. Boffi, C. Giusti and F. D. Pacati, Phys. Rep. **226**, 1 (1993).

[3] J.J. Kelly, Adv. Nucl. Phys. **23**, 75 (1996).

[4] J.P. McDermott, Phys. Rev. Lett. **65** 1991 (1990).

[5] J.M. Udías, P. Sarriguren, E. Moya de Guerra, E. Garrido and J.A. Caballero, Phys. Rev. C **48** 2731 (1993).

[6] Y. Jin, D.S. Onley and L.E. Wright, Phys. Rev. C **45** 1311 (1992).

[7] J.M. Udías, P. Sarriguren, E. Moya de Guerra and J.A. Caballero, Phys. Rev. C **53** R1488 (1996).

[8] J.A. Caballero, T.W. Donelly, E. Moya de Guerra and J.M. Udías, Nuc. Phys **A632** 323 (1998).

[9] B.D. Serot, Phys. Lett. **86B**, 146 (1979).

[10] C.J. Horowitz and B.D. Serot, Nuc. Phys. **A369** 503 (1981).

[11] C.J. Horowitz, D.P. Murdock and B.D. Serot, in *Computational Nuclear Physics*, edited by K. Langanke, J. A. Maruhn, and S. E. Koonin (Springer-Verlag, Berlin, 1991).

[12] A. Bouyssy, J.-F. Mathiot, Nguyen Van Giai, and S. Marcos, Phys. Rev. C **36**, 380 (1987).

[13] C. Fuchs, H. Lenske, and H.H. Wolter, Phys. Rev. C **52**, 3043 (1995).

[14] R. Fritz, H. Müther, and R. Machleidt, Phys. Rev. Lett **71**, 46 (1993).

[15] R. Brockmann and H. Toki, Phys. Rev. Lett **68**, 3408 (1992).

[16] R. Fritz and H. Müther, Phys. Rev. C **49**, 633 (1994).

[17] H.F. Boersma and R. Malfliet, Phys. Rev. C **49**, 233 (1994); **50**, 1253(E) (1994).

[18] T.W. Donelly, in: *Proceedings of the Workshop on Perspectives in Nuclear Physics at intermediate Energies*, edited by S.Boffi, C.C. degli Atti and M. Giannini, World Scientific, Trieste (1984).

[19] A. Picklesimer, J.W. Van Orden and S.J. Wallace, Physical Review C **32**, 1312 (1985).

[20] T.W. Donelly and A.S. Raskin, Ann. Phys. (N.Y.) **169**, 247 (1986).

[21] A. Picklesimer and J.W. Van Orden, Physical Review C **35**, 266 (1987).

[22] S. Boffi, C. Giusti and F.D. Pacati, Nuc. Phys. A **476**, 617 (1988).

[23] C. Giusti and F.D. Pacati, Nuc. Phys. A **476**, 617 (1988).

[24] A.S. Raskin and T.W. Donelly, Ann. Phys. (N.Y.) **191**, 78 (1989).

[25] A. Picklesimer and J.W. Van Orden, Physical Review C **40**, 290 (1989).

[26] R. Brockmann and R. Machleidt, Phys. Rev. C **42**, 1965 (1990).

[27] S. Haddad and M. Weigel, Phys. Rev. C **48**, 2740 (1993).

[28] T. de Forest, Nuc. Phys **A392** 232 (1983).

APPENDIX A

This section gives a survey of the explicit definitions for the relativistic bound state wave functions used in the present work. The solutions of the relativistic Hartree or Hartree-Fock equations are calculated in coordinate space and have the general structure

$$\Psi_\alpha(\boldsymbol{r}) = \left(\begin{array}{c} g_{nlj}^{m_\tau}(r) Y_{lj}^{m_j}(\Omega_r) \\ i f_{nl'j}^{m_\tau}(r) Y_{l'j}^{m_j}(\Omega_r) \end{array} \right) \chi^{m_\tau} . \tag{13}$$

$\alpha = \{n(ls)jm_j\tau m_\tau\}$ is an abbreviation for the various quantum numbers, where n denotes the radial quantum number, l the angular momentum, s the spin, j the coupled angular momentum, τ the isospin, m_j and m_τ the orientation of the coupled angular momentum and the isopin. The angular momentum of the lower component l' is given by the relation

$$l' = \left\{ \begin{array}{ll} l+1 & \text{for } l = j - 1/2 \\ l-1 & \text{for } l = j + 1/2 \end{array} \right\} \tag{14}$$

The normalization of the states is

$$\int d^3\boldsymbol{r} \, \Psi_\alpha^\dagger(\boldsymbol{r})\Psi_\alpha(\boldsymbol{r}) = \int_0^\infty r^2 dr \, \left(g_\alpha^2(r) + f_\alpha^2(r) \right) = 1 . \tag{15}$$

The Fourier transformation of the relativistic bound nucleon wave functions is given by

$$\Psi_\alpha(\boldsymbol{p}) = \frac{1}{(2\pi)^{3/2}} \int d^3\boldsymbol{r} \, e^{-i\boldsymbol{p}\cdot\boldsymbol{r}} \Psi_\alpha(\boldsymbol{r}) \tag{16}$$

which leads to the following explicit form of the bound state wave function in momentum space

$$\Psi_\alpha(\boldsymbol{p}) = \left(\begin{array}{c} (-i)^l \, g_{nlj}^{m_\tau}(p) \, Y_{lj}^{m_j}(\Omega_p) \\ i(-i)^{l'} \, f_{nl'j}^{m_\tau}(p) \, Y_{l'j}^{m_j}(\Omega_p) \end{array} \right) \chi^{m_\tau} , \tag{17}$$

where the real amplitudes $g_\alpha(p)$ and $f_\alpha(p)$ are defined according to

$$g_{nlj}^{m_\tau}(p) = \sqrt{\frac{2}{\pi}} \int_0^\infty r^2 dr \; j_l(pr) \, g_{nlj}^{m_\tau}(r)$$

$$f_{nl'j}^{m_\tau}(p) = \sqrt{\frac{2}{\pi}} \int_0^\infty r^2 dr \; j_{l'}(pr) \, f_{nl'j}^{m_\tau}(r) \tag{18}$$

and for the normalisation of the states it follows that

$$\int d^3\boldsymbol{p} \, \Psi_\alpha^\dagger(\boldsymbol{p}) \Psi_\alpha(\boldsymbol{p}) = \int_0^\infty p^2 dp \, \left(g_\alpha^2(p) + f_\alpha^2(p) \right) = 1 \; . \tag{19}$$

These momentum wave functions served as the input for the relativistic quasielastic electron scattering calculations. All calculations are performed in momentum space. Therefore, the momentum space wave functions were multiplied directly with the current operator and the Dirac spinor to obtain the matrix elements of the hadronic current.

		^{16}O		
	RH	RHF	RDDH	Exp.
$1s_{1/2}\,[MeV]$	-37.2	-38.6	-36.0	-40±8
$1p_{3/2}\,[MeV]$	-16.7	-18.0	-17.1	-18.4
$1p_{1/2}\,[MeV]$	-8.8	-10.6	-12.9	-12.1
$E/A\,[MeV]$	-5.56	-6.10	-7.82	-7.98
$R_{ch}\,[fm]$	2.75	2.74	2.75	2.73

TABLE I. The proton single particle energies [MeV] for the $1s_{1/2}$, $1p_{3/2}$ and $1p_{1/2}$ shells, the energy per nucleon (E/A) [MeV] and the rms charge radius R_{Ch} [fm] of ^{16}O for the relativistic Hartree (RH), the relativistic Hartree-Fock (RHF) and the relativistic density dependent Hartree (RDDH) approach. The calculated energy has been corrected to account for the effects of the spurious center of mass motion.

		^{16}O	
	RH	RHF	RDDH
I_L	2.83	2.83	2.81
I_T	3.30	3.31	3.12
I_{LT}	-2.43	-2.48	-2.13
I_{TT}	0.28	0.29	0.24

TABLE II. The integrated strength I_i of the various response functions in dimensionless variables. The values calculated according to Eq. (10) were multiplied by the factor 100.
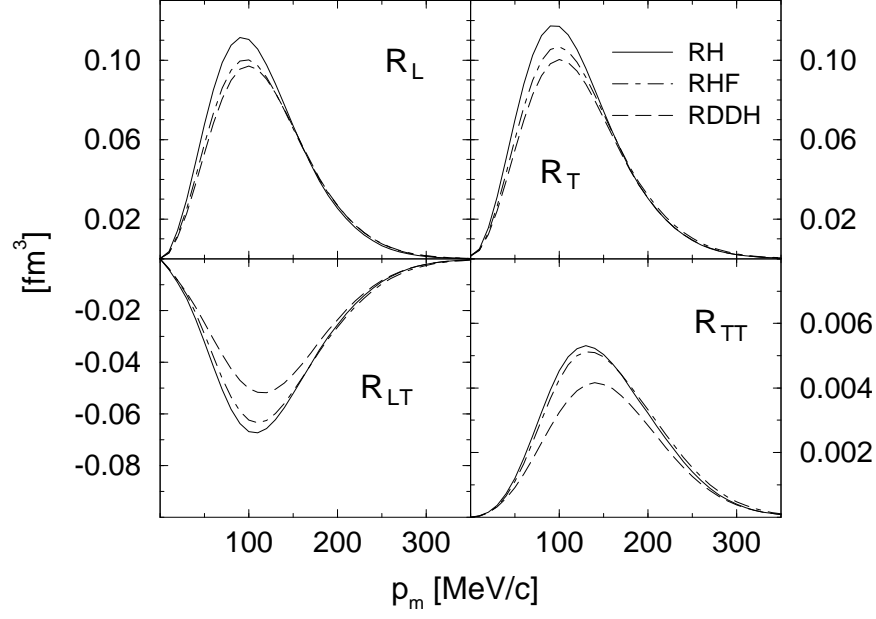
FIG. 1. Response functions R_L, R_T, R_{LT} and R_{TT} of Eq. (4) (in $[fm^3]$) as a function of the missing momentum p_m $[MeV/c]$. The solid line corresponds to the RH, the dash-dotted line to the RHF and the dashed line to the RDDH approach.
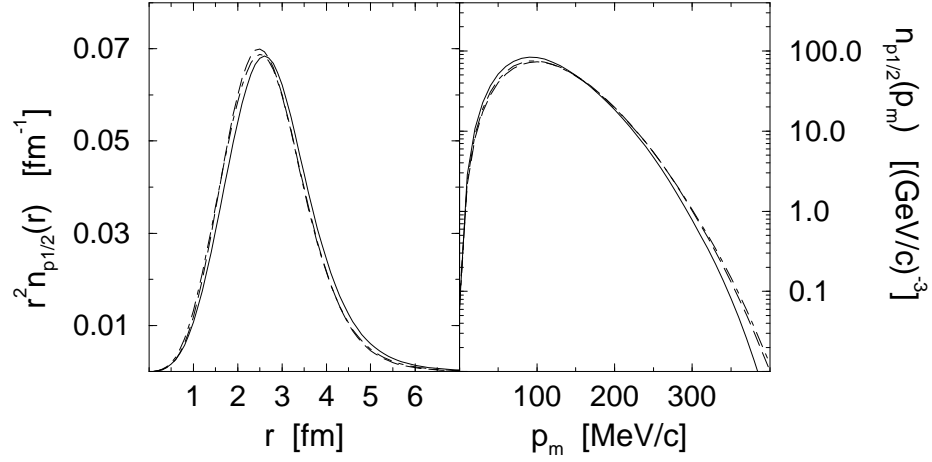

FIG. 2. Left panel: density distribution $r^2 n_{p1/2}(r)$ in $[fm^{-1}]$ as a function of the radius r ($[fm]$). Right panel: density distribution in momentum space $n_{p1/2}(p_m)$ in $[GeV/c^{-3}]$ as a function of the missing momentum. The lines are denoted as in Fig. 1.
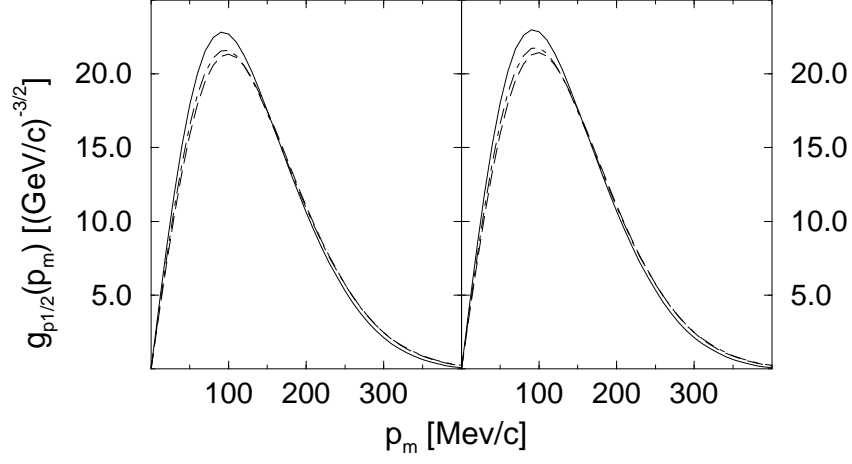
FIG. 3. Left Panel: upper component $g_{p1/2}(p_m)$ of the relativistic bound state wave function in $[(GeV/c)^{-3/2}]$ as a function of the missing momentum. Right panel: nonrelativistic limit $g_{p1/2}^{nr}(p)$. The lines are denoted as in Fig. 1.
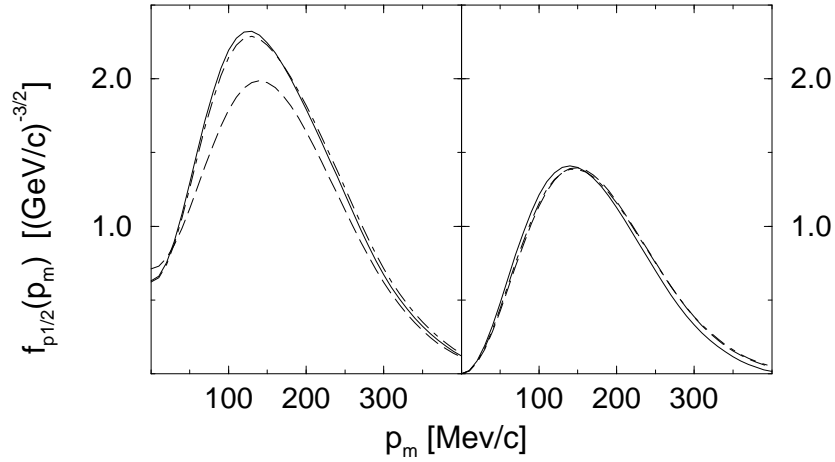

FIG. 4. Left panel: lower component $f_{p1/2}(p_m)$ of the relativistic bound state wave function in $[(GeV/c)^{-3/2}]$ as a function of the missing momentum. Right panel: nonrelativistic limit $f_{p1/2}^{nr}(p)$. The lines are denoted as in Fig. 1.
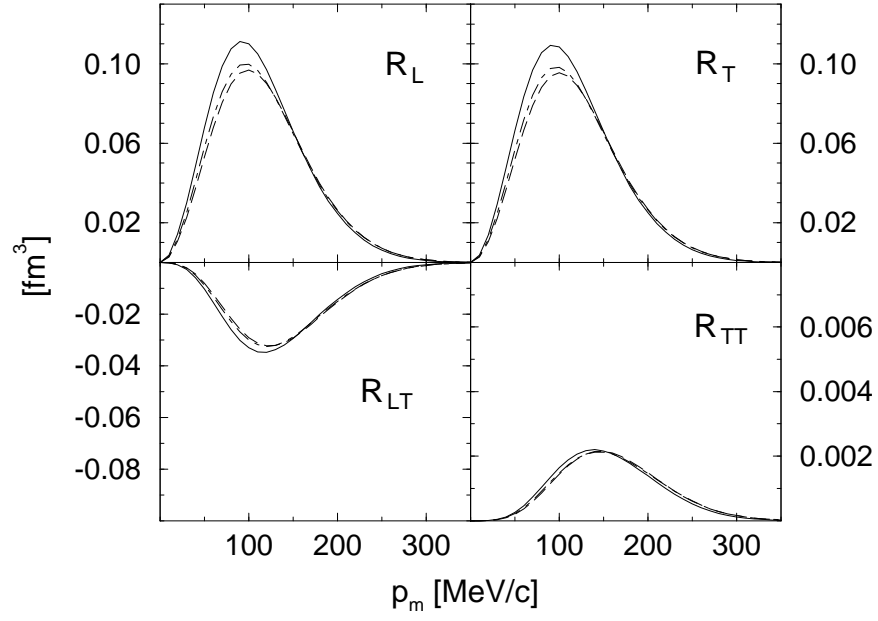
17

FIG. 5. Response functions in the nonrelativistic limit. The labelling is the same as in Fig. 1.